PCCP

Accepted Manuscript

ROYAL SOCIETY OF CHEMISTRY

www.rsc.org/pccp

View Article Online
DOI: 10.1039/C6CP01926A

Journal Name

ARTICLE

Synthesis, photophysical, electrochemical and electrochemiluminescent properties of A_2B_2 zinc porphyrins: effect of π–extended conjugation.

Received 00th January 20xx,
Accepted 00th January 20xx

DOI: 10.1039/x0xx00000x

www.rsc.org/

Elizabeth K. Galván-Miranda,[a] Hiram M. Castro-Cruz,[a] J. Arturo Arias-Orea,[a] Matteo Iurlo,[b] Giovanni Valenti,[b] Massimo Marcaccio,[b] and Norma A. Macías-Ruvalcaba†[a]

Synthesis of two A_2B_2 porphyrins, {5,15-bis-[4-(octyloxy)phenyl]-porphyrinato}zinc (II) (**4**) and {5,15-bis-(carbazol-3-yl-ethynyl)-10,20-bis-[4-(octyloxy)phenyl]-porphinato}-zinc (II) (**9**), is reported. The photophysical properties were studied by steady-state absorption and emission. Substituting the carbazolylethynyl moieties at two of the *meso* positions results in a large bathochromic shift of all the absorption bands, a notable increase on the absorption coefficient of the Q (0,0) band, and higher fluorescence quantum yield compared to porphyrin **4**, with two unsubstituted *meso* positions. Cyclic voltammetry and digital simulation show that electrogenerated radical ions of **9** are more stable than those of **4**. The lack of substituents at the *meso* positions of **4** leads to dimerization reactions of the radical cation. Despite this, annihilation reaction of **4** and **9** produces very similar electrogenerated chemiluminescence (ECL) intensity. Spectroelectrochemical experiments demonstrate that the electroreduction of **9** leads to a strong absorption band that might quench the ECL.

Introduction

The potential applications of porphyrins have made them attractive molecules in a wide range of research areas. They have been used for the development of a broad variety of sensors,[1] as catalysts,[2] in organic electronic devices,[3] in dye sensitized solar cells [4] and in bulk heterojunction cells,[5] where porphyrins are used for light harvesting as well as in energy and electron transfer.

Most of these applications rely on their rich photophysical and electrochemical properties, which can be fine-tuned by different substitution patterns on the ring periphery, incorporation of different metal ions in the core, or by axial ligand coordination to the incorporated metal.[6,7] It is known that aromatic substituents directly appended on the *meso*-positions of the porphyrin have little effect on the electronic properties of the molecule because the steric interactions between the porphyrin β-hydrogens and the aromatic unit do not allow for an efficient π overlap between the two.[8] To achieve the extended conjugation of porphyrin molecules, which translates into modification of their electronic properties, the incorporation of ethyne- or butadiyne- linkers has proved very successful. This strategy has been used in the synthesis of porphyrin-*yne*-porphyrin dimers, trimers or oligomers,[7,9,10] tetrakis(arylethynil)porphyrins,[11] and bis(arylethynyl)porphyrins (A_2B_2 and A_2BC types).[12–15] Bis(arylethynyl)porphyrins are particularly interesting for organic photovoltaics, OLED's development, and, in general, the organic electronics field.[14–17] As these applications usually involve electron transfer reactions, the study of porphyrins radical ion species is of major importance for this area.

Electrochemical techniques are powerful and versatile tools to investigate the formation and stability of radical cations and anions. The electrochemistry of porphyrins has been extensively studied, they usually show two one-electron oxidation and two one-electron reduction processes corresponding to the formation of radical cation, dication, radical anion, and dianion.[18] These radical ion species are fairly stable, especially in metallated porphyrins.[9,10,19] Such stability, along with their known emission properties, makes the porphyrins ideal candidates for electrogenerated chemiluminescence (also called electrochemiluminescence, ECL) studies.

Electrochemiluminescence arises from electron-transfer reactions of radical ion or ionic species generated at electrode surfaces; such reactions produce excited state molecules that emit light.[20] In the past few years, ECL applications and processes, including the mechanisms through which it takes place, have been reviewed;[21–23] yet, the investigation of some fundamental aspects, such as the correlation between structure and ECL properties, are still an active issue.[24]

[a] *Departamento de Fisicoquímica, Facultad de Química, Universidad Nacional Autónoma de México, Ciudad Universitaria, C.P. 04510, Ciudad de México, México.*
[b] *Department of Chemistry "G. Ciamician", University of Bologna, Via Selmi 2, 40126, Bologna, Italy.*
† nmaciasr@unam.mx

Electronic Supplementary Information (ESI) available: [additional experimental and simulated voltammograms, polymerization of porphyrin **4**, voltammograms for ECL experiments, ECL efficiency, and NMR spectra of porphyrin **9**]. See DOI: 10.1039/x0xx00000x

Even though the first report of ECL from porphyrins, by Bard, dates back to 1972,[25] there is a relatively small number of publications on this area. Most of the porphyrin-ECL publications involve highly phosphorescent Pt^{II} or Pd^{II} metalloporphyrins,[26–29] as well as to porphyrin-ruthenium complexes.[30,31] There are works carried out in aqueous media,[32,33] and more recently a zinc-porphyrin was used as a coreactant to induce the ECL emission of singlet oxygen instead of being the emitter.[34] Only the work of Sooambar *et al* [35] compares the effect of the *meso*- substituents on a porphyrin ring on its ECL properties.

In this work, we report the synthesis of {5,15-bis-(carbazol-3-yl-ethynyl)-10,20-bis-[4-(octyloxy)phenyl]-porphinato}-zinc (II) (**9**, Scheme 1) and a reference porphyrin without any arylethynyl substituents, {5,15-bis-[4-(octyloxy)phenyl]-porphyrinato}zinc (II) (**4**, Scheme 1)

A comprehensive study involving the optical characterization, cyclic voltammetry, UV-vis spectroelectrochemistry and ECL properties for these porphyrins is described. Digital simulation of the voltammograms allowed us to demonstrate that blocking the *meso* positions with the ethynylcarbazole substituents improves the stability of the radical ion species, but this does not necessarily translate into a more efficient ECL emission as there are other factors that need to be taken into consideration, such as the red-shifted absorption of the extended conjugation porphyrin and its corresponding radical species.

Results and discussion

Synthetic procedures

Two porphyrins, {5,15-bis-(carbazol-3-yl-ethynyl)-10,20-bis-[4-(octyloxy)phenyl]-porphinato}-zinc (II) (**9**) and {5,15-bis-[4-(octyloxy)phenyl]-porphyrinato}zinc (II) (**4**) were synthesized following the synthetic route depicted in Scheme 1 through minor modification of the procedures from the indicated references (see Experimental Section). Briefly, 5,15-bis-[4-(octyloxy)phenyl]-porphyrin (**3**) was obtained by reacting dipyrromethane (**1**) and 4-octyloxybenzaldehyde (**2**) in presence of TFA and using DDQ to oxidize the porphyrinogen. Then, porphyrin **3** was treated with $Zn(OAc)_2$ to afford the Zn-metallated porphyrin **4**, a change in color, from deep purple to bright pink, as well as a decrease in the number of Q bands of the absorption spectrum indicated that metal incorporation was successful. Once metallated, the two free *meso* positions were brominated by treatment with NBS yielding porphyrin (**5**). On the other hand, 3-ethynylcarbazole (**8**) was obtained from carbazole by a succession of steps involving the iodination of carbazole followed by a Sonogashira coupling with trimethylsylil acetylene and desilylation of the latter. The final step involved a copper-free Sonogashira coupling of **5** and **8** to obtain **9**.

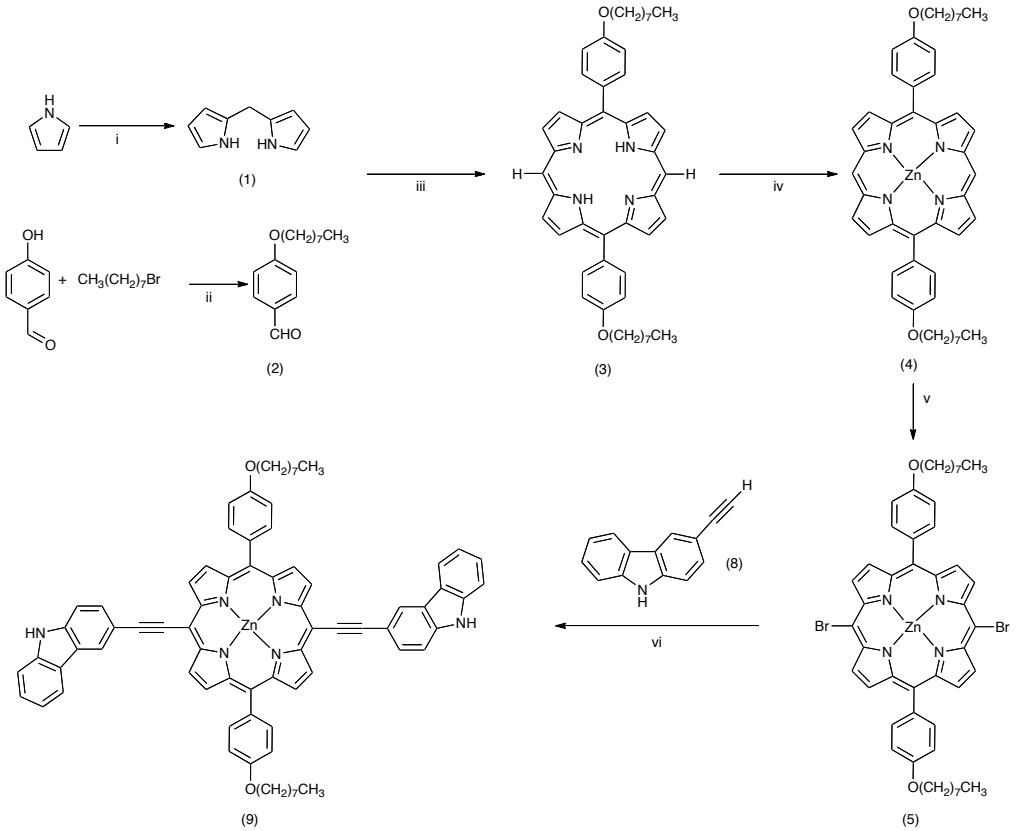

Scheme 1 Synthesis of porphyrin **9**. i) Paraformaldehyde, $InCl_3$, 50 °C, N_2 atmosphere. ii) K_2CO_3, DMF, 100 °C. iii) TFA, CH_2Cl_2, N_2 atmosphere, dark, then DDQ and TEA. iv) $Zn(OAc)_2$, DMF, reflux. v) NBS, $CHCl_3$, 0 °C. vi) $Pd(dba_2)_3$, P(*o*-tol)$_3$, TEA, THF, 30 °C, N_2 atmosphere.

View Article Online
DOI: 10.1039/C6CP01926A

Voltammetric Analysis

The electrochemical behavior of **4** and **9** was studied by cyclic voltammetry in Bu_4NPF_6 0.1 M /THF at –5 °C. The voltammetric curves of the two porphyrins, recorded at 0.1 V/s, are shown in Fig. 1 and 2. On the anodic scan, two oxidation processes are observed for both **4** and **9** (Fig. 1). Voltammograms encompassing only the first oxidation peak show that it is a reversible or quasi-reversible process; this signal has been attributed to the one-electron oxidation yielding the corresponding radical cation. The potential of the first oxidation peak of **9** is about 0.12 V less positive than that of **4**, and qualitatively the reversibility of the process suggests that the radical cation of **9** is more stable than that of **4**. These observations can be explained by the extended π-conjugation of **9**. On the other hand, the second oxidation, which leads to the formation of the dication, is an irreversible process for **4**, and slightly reversible for **9**. On the negative potential sweep, two reduction signals are observed for each porphyrin (Fig. 2), at approximately –2.01 and –2.43 V for **4** and –1.69 and –2.19 V for **9**. These peaks are attributed to consecutive one-electron reductions, yielding the corresponding radical anion and dianion.

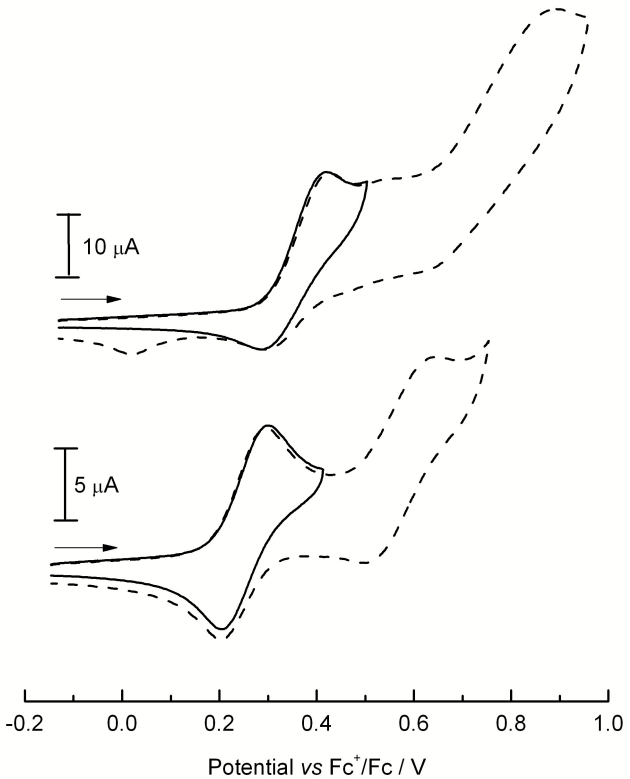

Fig. 1 Experimental anodic scan of: 1.21 mM **4** (top) and 1.19 mM **9** (bottom) encompassing only the first (solid), and first and second (dashed) oxidation processes at 0.1 V/s in THF containing 0.1 M Bu_4NPF_6 at –5 °C at a glassy carbon working electrode.

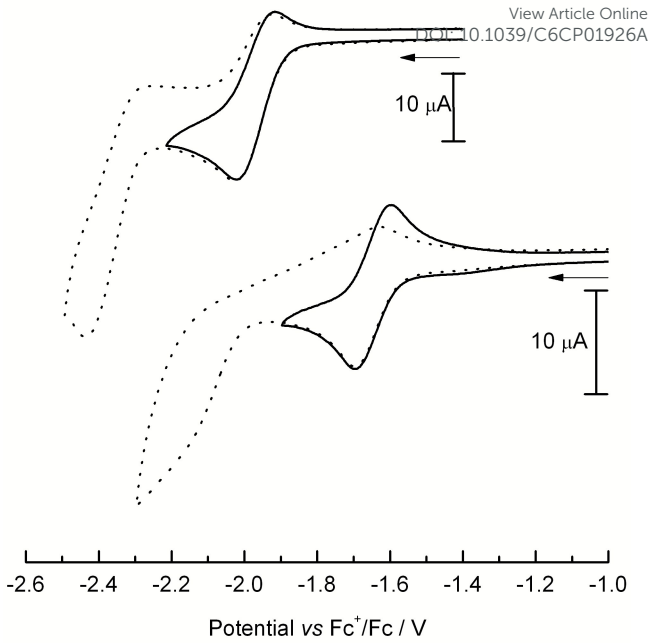

Fig. 2 Experimental cathodic scan of: 1.21 mM **4** (top) and 1.19 mM **9** (bottom) encompassing only the first (solid), and first and second (dashed) reduction processes at 0.1 V/s in THF containing 0.1 M Bu_4NPF_6 at –5 °C at a glassy carbon working electrode.

Experimental voltammograms encompassing only the first oxidation peak were recorded for scan rates ranging from 0.1 to 1.0 V/s and concentrations between about 0.4 and 1.2 mM, and the voltammograms were analyzed by digital simulation. The analysis of this peak was based in terms of the reversible oxidation of the porphyrin to its radical cation, reaction 1. In order to account for the loss of reversibility, a bimolecular dimerization of the radical cation was initially tested (reaction 2). This reaction scheme allowed quite acceptable agreement at all scan rates and concentrations for **4**, but not for **9**. The latter needed large increases in the value of $k_{f,2}$ as the concentration of porphyrin decreased (200 $M^{-1}s^{-1}$, 1.19 mM; 500 $M^{-1}s^{-1}$, 0.67mM; 700 $M^{-1}s^{-1}$, 0.4 mM). This nonconstant rate constant means that the proposed reaction scheme is inadequate for **9**; therefore, reaction 2 was replaced by a first-order decomposition of the radical cation (reaction 3). This mechanism was found to fit well for all of the voltammetric data of **9**.

$P \rightarrow P^{\bullet+} + e^-$	$E^\circ_1, k_{s,1}, \alpha_1$	(1)
$2\ P^{\bullet+} \rightarrow PP^{2+}$	$K_2, k_{f,2}, k_{b,2}$	(2)
$P^{\bullet+} \rightarrow$ Prod	$K_3, k_{f,3}, k_{b,3}$	(3)

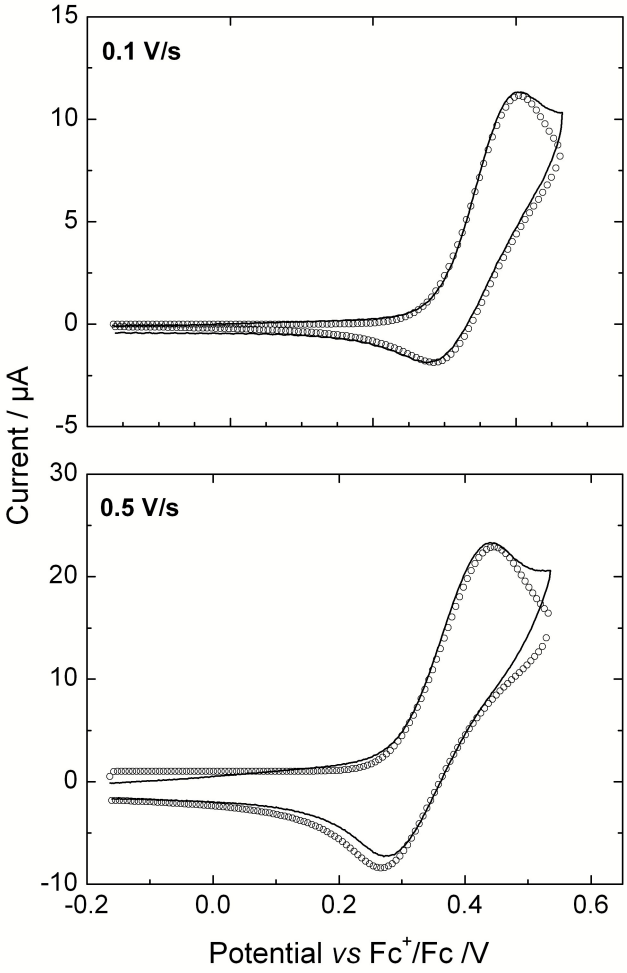

Fig. 3 Background-corrected experimental voltammograms of 0.65 mM **4** in THF with 0.1 M Bu_4NPF_6 (black solid line). Simulation based on reactions 1 and 2 (open circles) with parameter values according to Table 1. Additional voltammograms for 1.20 mM on ESI, Fig. 1S.

It was also demonstrated that for **4**, the first order decomposition of the radical cation does not account for the experimental data. In this case it was observed that there was not a unique $k_{f,3}$ value that fitted all the scan rates, it was necessary to increase the rate constant as the scan rate increased. Summarizing, while for porphyrin **4** the chemical reaction following the formation of the radical cation was well accounted for by a second-order dimerization reaction, for **9**, a first-order reaction provided good fits. The simulation parameters used to fit the voltammograms are listed in Table 1, and examples of the fits to the data are shown in Figs. 3, 4, 1S and 2S.

We next focused our attention on the analysis of the first reduction process of **4** and **9**. In the same way, voltammograms recorded at different porphyrin concentrations and scan rates, from 0.1 to 1.0 V/s, were analyzed by digital simulation. The fit of this reduction process was treated as the reversible formation of the radical anion (reaction 4); and to account for the experimentally observed

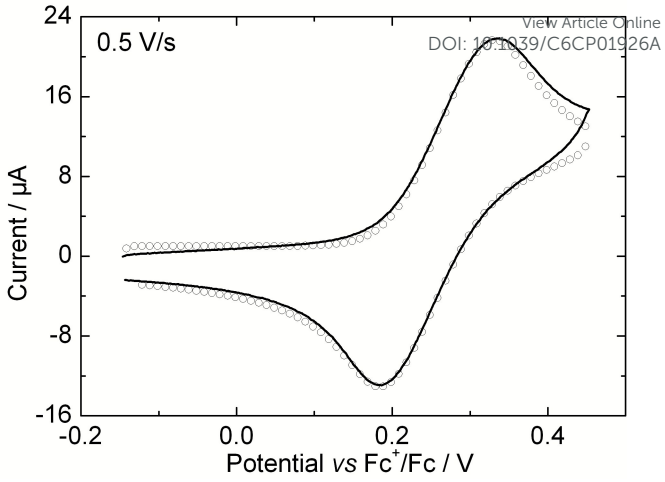

Fig. 4 Background-corrected experimental voltammograms of 1.19 mM **9** in THF with 0.1 M Bu_4NPF_6 (black solid line). Simulation based on reactions 1 and 3 (open circles) with parameter values according to Table 1. Additional voltammograms on ESI, Fig. 2S.

loss of reversibility, again two different reactions were tested: the bimolecular dimerization of the radical anion (reaction 5), and the first-order decomposition of the radical anion (reaction 6).

$P + e^- \rightarrow P^{\bullet -}$	$E°_4$, $k_{s,4}$, α_4	(4)
$2P^{\bullet -} \rightarrow PP^{2-}$	K_5, $k_{f,5}$, $k_{b,5}$	(5)
$P^{\bullet -} \rightarrow$ Prod	K_6, $k_{f,6}$, $k_{b,6}$	(6)

We proved that for both porphyrins, the reaction scheme consisting of reactions 4 and 5 was inadequate. In both cases, it was necessary to increase the $k_{f,5}$ value as the concentration of the porphyrin decreased. On the other hand, the reaction scheme involving the first-order decomposition of the radical anion provided acceptable fits for all the scans and concentrations studied. The best-fit simulation parameter values for the first reduction process are included in Table 2. Examples of the fits to the experimental voltammograms are shown in Figs. 5, 6, and 3S.

Table 1. Simulation parameter values for the oxidation of **4** and **9** in THF / 0.1 M Bu_4NPF_6 at –5 °C[a]

Por	C/mM	$E°_1$/V	$k_{s,1}$/cm s^{-1}	K_2	$k_{f,2}/M^{-1}s^{-1}$	D/cm^2s^{-1}
		$P \rightarrow P^{\bullet +} + e^-$ (1)		$2P^{\bullet +} \rightarrow PP^{2+}$ (2)		
4	1.20	0.34	0.0064	1×10^7	2.2×10^3	7.58×10^{-6}
	0.90	0.33	0.0060	1×10^7	2.2×10^3	7.60×10^{-6}
	0.65	0.34	0.0070	1×10^7	2.3×10^3	7.84×10^{-6}
				K_3	$k_{f,3}$ /s^{-1}	
				$P^{\bullet +} \rightarrow$ Prod (3)		
9	1.19	0.25	0.010	1×10^7	0.21	1.50×10^{-6}
	0.67	0.25	0.010	1×10^7	0.23	1.58×10^{-6}
	0.40	0.25	0.015	1×10^7	0.19	1.56×10^{-6}

[a] Potentials are referred to the formal potential of the ferrocenium/ ferrocene couple. Diffusion coefficients of all species were set equal to the value shown in the table. Solution resistance: 2000 Ω was electronically compensated; remaining 1500 Ω was introduced into the simulation.

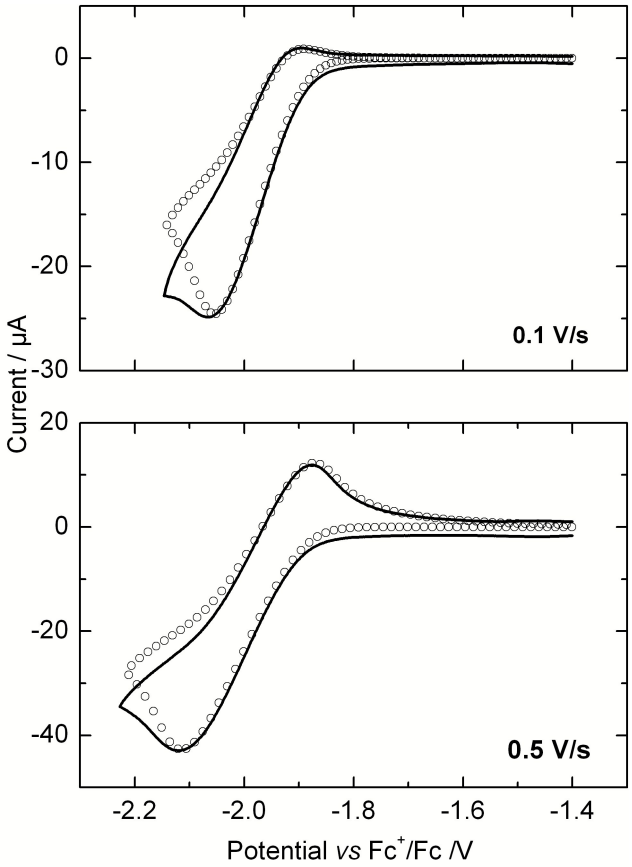

Fig. 5 Background-corrected experimental voltammograms of 1.90 mM **4** in THF with 0.1 M Bu_4NPF_6 (black solid line). Simulation based on reactions 4 and 6 (open circles) with parameter values according to Table 2.

Table 2. Simulation parameter values for the first reduction process of **4** and **9** in THF / 0.1 M Bu_4NPF_6 at –5 °C[a]

Por	C/mM	$E°_1$ / V	$k_{s,4}$ / cm s^{-1}	K_6	$k_{f,6}$ /$M^{-1}s^{-1}$	D/cm^2s^{-1}
		P + e^- → $P^{\bullet-}$(4)		$P^{\bullet-}$ → Prod (6)		
4	1.90	–1.96	0.009	1×10^7	1.35	4.30×10^{-6}
	1.13	–1.95	0.009	1×10^7	1.38	4.90×10^{-6}
9	1.19	–1.64	0.030	1×10^7	0.10	1.50×10^{-6}
	0.67	–1.64	0.029	1×10^7	0.10	1.58×10^{-6}
	0.40	–1.64	0.030	1×10^7	0.11	1.56×10^{-6}

[a] Potentials are referred to the formal potential of the ferrocenium/ ferrocene couple. Diffusion coefficients of all species were set equal to the value shown in the table. Solution resistance: 2000 Ω was electronically compensated; remaining 1500 Ω was introduced into the simulation.

The most notable feature on the parameters shown in Tables 1 and 2 is that the diffusion coefficient used to fit the voltammograms of porphyrin **4** reduction process is about 1.7 times smaller than the coefficient used to fit the oxidation. The need to use so different diffusion coefficient values led us to think that the first oxidation process might involve a more complex mechanism, which would result in higher current values, meaning that probably more than one electron is involved. Consequently, a re-evaluation of the digital simulation of the electrochemical oxidation process of **4** was needed. To explain the higher current values, there is the possibility that the dimer formed in reaction 2 is oxidized at the same, or even lower, potential than the neutral porphyrin.

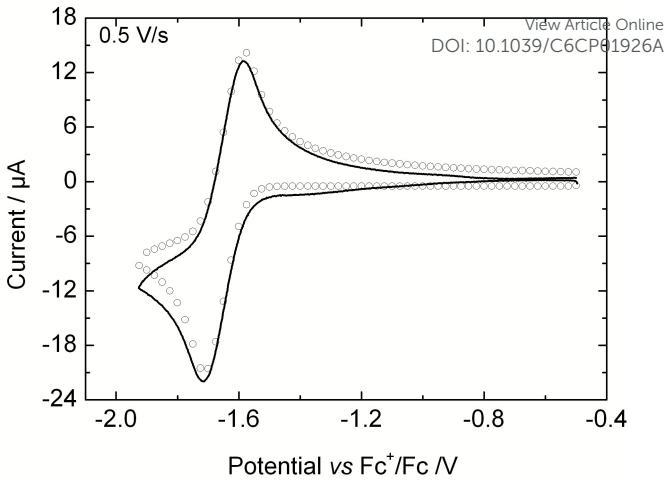

Fig. 6 Background-corrected experimental voltammograms of 1.20 mM **9** in THF with 0.1 M Bu_4NPF_6 (black solid line). Simulation based on reactions 4 and 6 (open circles) with parameter values according to Table 2. Additional voltammograms on ESI, Fig. 3S.

This assumption makes sense since a dimer, due to its increased conjugation, would be easier to oxidize than the monomer. To test this hypothesis, we added to the simulation program a fast deprotonation reaction of the PP^{2+} dimer to form a neutral dimer (reaction 7), along with the one-electron oxidation of the dimer leading to a dimer radical cation (reaction 8). Reaction 7 was treated as extremely fast and irreversible, so that the rate-limiting step is the dimerization, reaction 2. The diffusion coefficient was kept close to the value used for the reduction process, so that the height of the peak and the reversibility degree were controlled by the rate constant value of reaction 2.

$PP^{2+} \rightarrow PP + 2H^+$ K_7, $k_{f,7}$, $k_{b,7}$ (7)

$PP \rightarrow PP^{\bullet+} + e^-$ $E°_8$, $k_{s,8}$, α_8 (8)

Simulations according to this reaction scheme (reactions 1-2,7-8) are in good agreement with the experimental voltammograms recorded at different scan rates and concentrations.

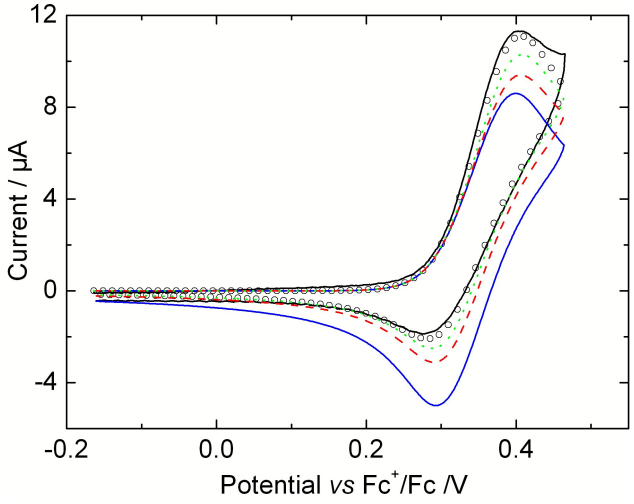

Fig. 7 Background corrected experimental voltammogram of 0.65 mM **4** at 0.1 V/s (black solid line) and best-fit simulation (open circles, $k_{f,2}$ =7×$10^3$$M^{-1}s^{-1}$) according to parameters values summarized in Table 3. Influence of the magnitude of $k_{f,2}$: 3×10^3 $M^{-1}s^{-1}$ (green dotted line), 1×10^3 $M^{-1}s^{-1}$ (red dashed line) and without dimerization reaction (blue solid line).

View Article Online
DOI: 10.1039/C6CP01926A

Table 3. Simulation parameter values for the oxidation peak of **4** in THF / 0.1 M Bu_4NPF_6 at –5 °C[a].

Concentration	0.65 mM			1.20 mM		
Electrochemical Reactions	$E°_1$ / V	α	k_s / cm s^{-1}	$E°_1$ / V	α	k_s / cm s^{-1}
$P \rightarrow P^{\bullet+} + e^-$	0.34	0.5	6.5×10^{-3}	0.35	0.5	6.0×10^{-3}
$PP \rightarrow PP^{\bullet+} + e^-$	0.33	0.5	0.016	0.33	0.5	0.016
Chemical reactions	K	k_f	k_b	K	k_f	k_b
$2P^{\bullet+} \rightarrow PP^{2+}$	1.0×10^{7}	7.0×10^{3}	7.0×10^{-4}	1.0×10^{7}	7.0×10^{3}	7.0×10^{-4}
$PP^{2+} \rightarrow PP$	1.0×10^{7}	1.0×10^{9}	100	1.0×10^{7}	1.0×10^{9}	100
D/cm^2s^{-1}	4.8×10^{-6} all species			4.5×10^{-6} all species		

[a] The same values were used to fit all scan rates from 0.1 to 1.0 V/s. First-order constants in s^{-1} and second-order constants in $M^{-1}s^{-1}$. 2000 Ω of solution resistance was electronically compensated, and the remaining 1500 Ω was applied in the simulation.

As shown in Fig. 7, simulations were very sensitive to the $k_{f,2}$ value. However, any $k_{f,2}$ value larger than 7.0×10^3 did not improve the already good fitting. This means that $k_{f,2}$ must be at least 7.0×10^3 $M^{-1}s^{-1}$ but simulation does not allow to determine the exact value. The agreement of simulations using this reaction scheme was as good as with the scheme involving only reactions 1 and 2, it was only the discrepancy between the diffusion coefficients that allowed us to discriminate between these two reaction pathways. Simulation parameters that provided the best agreement to the experimental data of different concentrations are given in Table 3, and examples of the fit to the experimental data are shown in Fig. 8, and 4S.

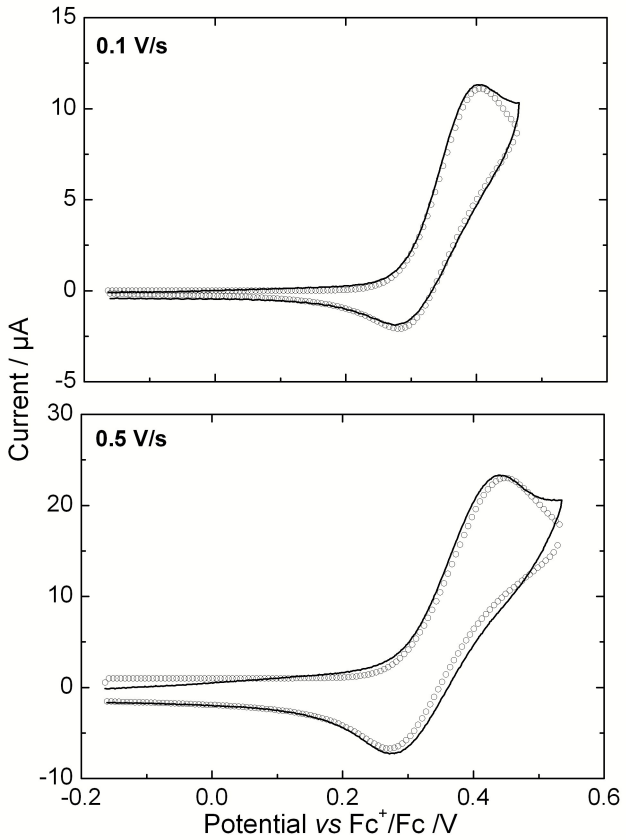

Fig. 8 Background-corrected experimental voltammograms of 0.65 mM **4** in THF with 0.1 M Bu_4NPF_6 (black solid line). Simulation based on reactions 1-2, 7 and 8 (open circles) with parameter values according to Table 3. Additional voltammograms on ESI, Fig. 4S.

The reaction scheme depicted in Table 3 for porphyrin **4** is consistent with the initial steps for anodic polymerization, which involves the dimerization of the molecule and further oxidation of the dimer. Potentiostatic electropolymerization of **4** was achieved for 10 mM solutions in Bu_4NPF_6 0.1 M /THF at –5 °C when a potential step at the value corresponding to the first oxidation was applied. After the electrolysis, a porphyrin film is deposited on the electrode (Fig. 5S, ESI); similar experiments using a large area Pt electrode yielded a dark purple solid that has an UV-vis absorption spectrum (Fig. 6S, ESI) similar to that reported for *meso-meso* porphyrin dimers and trimers. [36,37] Formation of dimers, oligomers or polymers is expected as **4** has two unhindered *meso* positions where coupling can occur.[38]

Photophysical Properties

The absorption spectra of **4** and **9** were recorded in THF at room temperature (Fig. 9), their optical properties are summarized in Table 4. They both present the spectral characteristics of Zn-metallated porphyrins.[39,40] Increasing the conjugation of the porphyrin macrocycle by functionalization of the *meso*- positions (5- and 15- positions) with ethynylcarbazol substituents produces a bathochromic shift in both the Q and Soret (B) bands (*ca*. 2200 cm^{-1}). These large red shifts indicate the modification of the conjugation pathway that allows an effective electronic communication between the carbazole moiety and the porphyrin core.[11,41] The relative intensities of the Q(0,0), and Q(1,0) bands, also known as α and β bands respectively, change upon functionalization with the ethynylcarbazole substituents; while for porphyrin **4** the β band is more intense than the α band, for **9** the α band is more intense than the β band and has larger extinction coefficients than **4**. The notable increase in intensity of the lower energy Q band (ε= 62000 $M^{-1}cm^{-1}$) and the broad Soret band (FWHM of 859 cm^{-1}) have been reported before for other *meso*- arylethynyl substituted porphyrins and are due to the loss of degeneracy of the porphyrin e_g symmetry LUMO.[12,42,43] Fig. 9 also shows the steady-state emission spectra of the porphyrins under study. The spectra were obtained by the excitation at the λ_{max} of the Soret band and show the emission corresponding to the decay from the first excited state to two vibrational states of the ground state, Q(0,0) and Q(0,1).[44]

View Article Online
DOI: 10.1039/C6CP01926A

Table 4. Spectroscopic data of **4** and **9**

Por	λ_{abs} / nm	ε / 10^5 $M^{-1}cm^{-1}$	λ_{em} / nm	E_s / eV [a]	Φ_{lum} [b]	λ_{em} / nm [c]	Φ_{ECL} [d]
4	414, 544, 581	3.36, 0.15, 0.04	588, 638	2.12	0.029	623	0.019
9	459, 617, 668	3.43, 0.11, 0.62	676, 739	1.84	0.088	701, 752	0.012

[a] $E_s = hc\,(\bar{\nu}_{abs} + \bar{\nu}_{em})/2$ [45,46] [b] $\Phi_{[Ru(bpy)3](PF6)2}$= 0.095 in CH_3CN.[47] [c] Obtained with BPO as coreactant. [d] $\Phi_{[Ru(bpy)3](PF6)2}$= 0.05

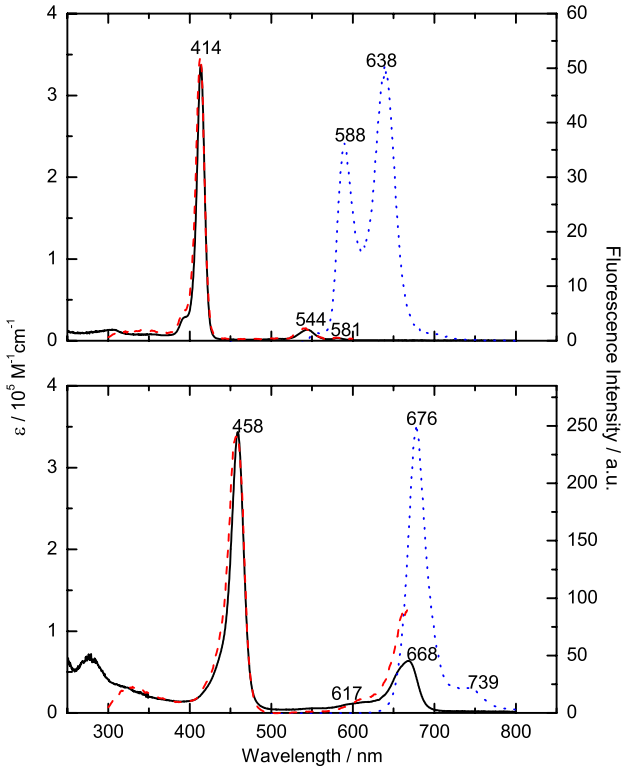

Fig. 9 Absorption (black solid line), emission (blue dotted line) and excitation (red dashed line) spectra for **4** (top, λ_{exc}= 414 nm, λ_{det}= 638 nm) and **9** (bottom, λ_{exc}= 458 nm, λ_{det}= 677 nm) in THF.

Consistent with the absorption spectra, emission bands of **9** are also red shifted when compared to **4** (Table 4). Porphyrin **4** spectrum is very similar to that of ZnTPP, [44,48] while **9** spectrum has similar features than those reported for *bis*-trimethylsilylethynyl and *meso*-arylethynyl porphyrins.[11,42] Fluorescence quantum yields increase as the conjugation increases; data is summarized in Table 4. The excitation spectra recorded at the λ of maximum emission match the absorption spectra for each porphyrin (Fig. 9).

Electrogenerated Chemiluminescence

The energy feasibility of the radical ion annihilation reaction ($\Delta H°$) was calculated from the half-wave redox potentials corresponding to the first one-electron oxidation ($E^{\circ}_{P^+/P}$) and reduction (E°_{P/P^-}) processes using equation 1.[20,49]

$$\Delta H° = E^{\circ}_{P^+/P} - E^{\circ}_{P/P^-} - 0.1\ eV \qquad (1)$$

The estimated enthalpies ($\Delta H°$= 2.29 and 1.85 eV for **4** and **9**, respectively), obtained from the experimental voltammograms (Fig. 7S, ESI), indicate that the annihilation reaction (reaction 9) produces enough energy to populate the first excited state (S_1). The energy of the first excited state (E_s), calculated as the average between the λ_{max} of the the Q(0,0) absorption and emission bands, [45,46] is also reported in Table 4. Since digital simulation results show that the radical ions of both porphyrins are fairly stable, and the $\Delta H°$ is larger than the E_S, ECL measurements by direct radical cation-radical anion annihilation were performed. First, the experiments were performed by stepping the potential of the working electrode about 30 mV beyond the peak potential for the one-electron oxidation and reduction of the porphyrins, and alternating between these two values. Current and photocurrent signals were simultaneously monitored and plotted as a function of time. Fig. 10 shows that under these conditions ECL emission was observed for **4** and **9**. The mechanism for the ECL generation is depicted in reactions 1, 4, 9, and 10.

$$P \rightarrow P^{\bullet+} + e \qquad (1)$$
$$P + e \rightarrow P^{\bullet-} \qquad (4)$$
$$P^{\bullet+} + P^{\bullet-} \rightarrow P^* + P \qquad (9)$$
$$P^* \rightarrow P + h\nu \qquad (10)$$

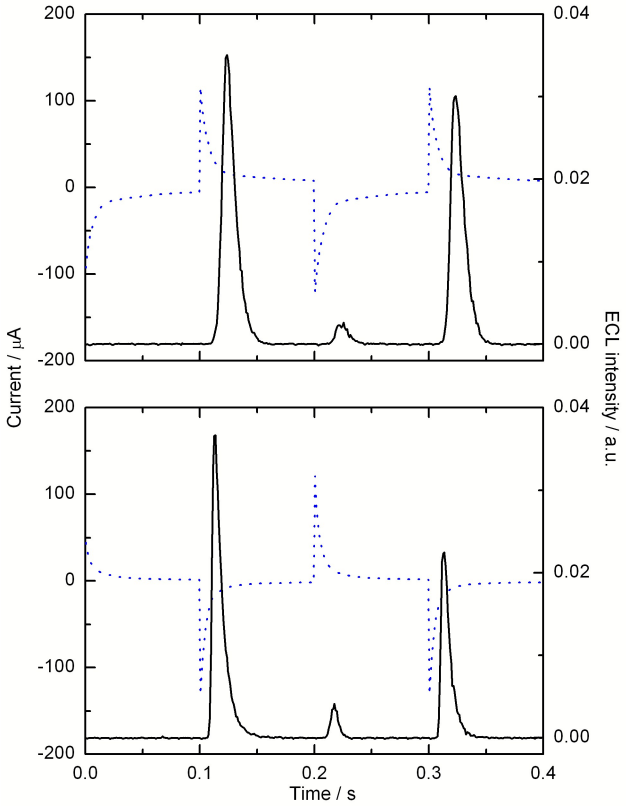

Fig. 10 Current (blue dotted line) and ECL intensity (black solid line) in 0.05 M Bu_4NPF_6/THF at platinum electrode for: porphyrin **4**, voltage pulsing between -2.2 V and +0.8 V vs Ag, pulse width = 0.1 s, ECL current range: 000.0 μA (top); porphyrin **9**, voltage pulsing between +0.8 V and -1.6 V vs Ag, pulse width = 0.1 s, ECL current range: 000.0 μA (bottom). PMT bias: 750 V.

View Article Online
DOI: 10.1039/C6CP01926A

It is interesting to note that upon pulsing the potential back and forth between the first reduction and the first oxidation of the porphyrin, the intensity of the ECL transients is not symmetric, even though the current-time curves display a symmetric behavior. As seen in Fig. 10 (top), for porphyrin **4** the ECL emission is more intense for the oxidation than for the reduction step. The opposite is observed for **9** where the ECL is more intense on the reduction step (Fig. 10 bottom). These anomalous or asymmetrical ECL transients have been reported before and they can be due to side reactions *e.g.* dimerization.[50–54] Simulation results for **4** show that the radical cation undergoes dimerization reaction that could further lead to the formation of polymeric or oligomeric films (*vide supra*), this could account for the asymmetric transients observed in Fig. 10. For **9** the electrochemical simulation results show that both the radical anion and radical cation undergo unimolecular decomposition with similar reaction rates (Tables 1 and 2), hence, emission of equal intensity is expected upon both oxidizing and reducing steps. A possible explanation for the asymmetric ECL transients (Fig. 10 bottom) is that there is some species that somehow quenches the emission. Evidently this is a very complex system that involves many different factors, and requires further studies that are out of the scope of this work. On the other hand, although the photoluminescence quantum yield of **9** is three times higher than that of **4**, the ECL efficiency is very similar for the two porphyrins (Table 4); this effect is likely due to the small Stokes shift for **9** that increases the self-absorption typical of ECL experimental conditions.

Furthermore, the ECL emission for the two porphyrins was also obtained in a so-called "reductive oxidation" mechanism using benzoyl peroxide (BPO) as coreactant. Fig. 11 (top) shows the cyclic voltammogram of a solution containing **4** and an excess of BPO. During the sweep, BPO is reduced to $BPO^{\bullet-}$; this is followed by a fast reaction to produce benzoate anion, $C_6H_5CO_2^-$, and benzoate radical, $C_6H_5CO_2^\bullet$ (reactions 11-12), which is a strong oxidizing agent.[46] $C_6H_5CO_2^\bullet$ can easily oxidize the electrochemically generated $P^{\bullet-}$ to its excited state P*, thus resulting in a strong ECL signal (reactions 13-14, 10). When the electrode potential approaches the second reduction of the porphyrin (around -2.4 V vs Ag), the ECL signal shows a second increase in intensity. This can be accounted for by a comproportionation reaction of the porphyrin dianion, which generates more radical anion [55,56] (reaction 15) that reacts with $C_6H_5CO_2^\bullet$ increasing the concentration of P*.

$$BPO + e^- \rightarrow BPO^{\bullet-} \quad (11)$$
$$BPO^{\bullet-} \rightarrow C_6H_5^- + C_6H_5CO_2^\bullet \quad (12)$$
$$P + e^- \rightarrow P^{\bullet-} \quad (13)$$
$$P^{\bullet-} + C_6H_5CO_2^\bullet \rightarrow P^* + C_6H_5CO_2^- \quad (14)$$
$$P^* \rightarrow P + h\nu \quad (10)$$
$$P^{2-} + P \rightarrow 2P^{\bullet-} \quad (15)$$
$$P^{2-} + C_6H_5CO_2^\bullet \rightarrow P^{\bullet-} \quad (16)$$

As shown in Fig. 11 (bottom), the simultaneous reduction of **9** and BPO also produces luminescence but the pattern is different than that of **4**. In fact, the ECL signal can only be observed when the second reduction of the porphyrin is reached thus the ECL emission may be due to the oxidation of the dianion by the benzoate radical (reaction 16); however this emission is very low because the second reduction of **9** is completely irreversible thus only a small fraction of **9** is available for reaction 16, also the irreversibility renders the comproportionation mechanism not possible.

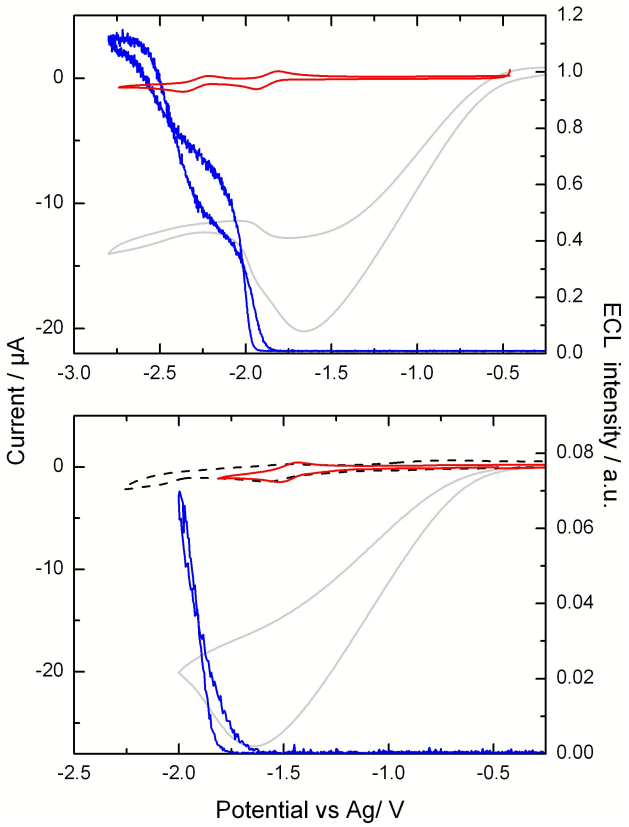

Fig. 11 Cyclic voltammogram (grey solid line) and ECL intensity (blue solid line) of **4** (top) and **9** (bottom) in presence of an excess BPO (20 times) in 0.05 M Bu_4NPF_6/THF at platinum electrode. Scan rate: 0.1 V/s. PMT bias 750 V. ECL current range: 0.0 µA. Cyclic voltammograms of **4** (red solid line) and **9** (red solid and black dashed line) are shown for comparison.

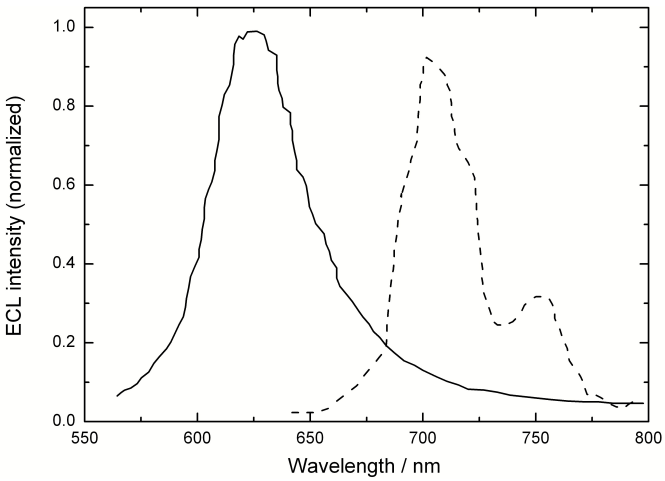

Fig. 12 ECL spectra for **4** (solid) and **9** (dashed) in THF. PMT bias 750 V, integration time 1000 ms, step 2 nm.

ECL spectra for both porphyrins were recorded by annihilation, pulsing the potential between the first oxidation and the first reduction, and by coreactant. The ECL spectra with BPO are presented in Fig. 12; they are very similar to their corresponding photoluminiscence spectrum (Fig. 9), indicating that the emissive species in ECL are the same as for the photoluminescence. The red shift is due to experimental factors such as the difference in slit widths, different instruments for recording the spectra and self-absorption as a result of the high concentration on the ECL measurements.[57]

Spectroelectrochemistry

In order to evaluate the spectral evolution of the radical ionic species of the porphyrins, thin-layer spectroelectrochemistry experiments were performed. Due to the high extinction coefficient of the Soret band of the porphyrins, spectroelectrochemical experiments were performed at low concentrations (20 μM).

For the formation of the radical cation species, the potential was stepped approximately 100 mV beyond the oxidation peak. Spectra of **4** show that the intensity on the Soret band decreases significantly during the electrolysis and a new band of lower intensity appears at 450 nm (Fig. 13A). Evolution of the spectra of **9** (Fig. 13C) displays a considerable decrease in the intensity of both the Soret, 459 nm, and the Q (0,0) band, 668 nm; the absorption intensity seems to increase at lower energies but a band cannot be defined.

To allow for a more detailed analysis of the lower energy bands, a second set of experiments, with high concentration solutions (*ca.* 0.5 mM), was performed. Electrolysis of **4** (Fig. 13B) results in a slight decrease of the Q (1,0) band at 544 nm, an increase of the Q (0,0) band at 581 nm, and the appearance of the new band at around 450 nm that was also evident at lower concentration; no additional bands emerge. For **9** (Fig. 13D), additional to the decrease on both the Soret and Q (0,0) bands, a broad band between 705 and 915 nm becomes evident. The behavior exhibited by **4** is very similar to that reported for the electropolymerization of a magnesium porphine,[38] and is consistent with the results from digital simulation, electrolysis, and ECL where the formation of a polymeric or oligomeric film is proposed (*vide supra*). On the other hand, the weakened Soret band and the broad diffuse band around 810 nm of **9** can be attributed to the presence of the porphyrin radical cation.[58–60]

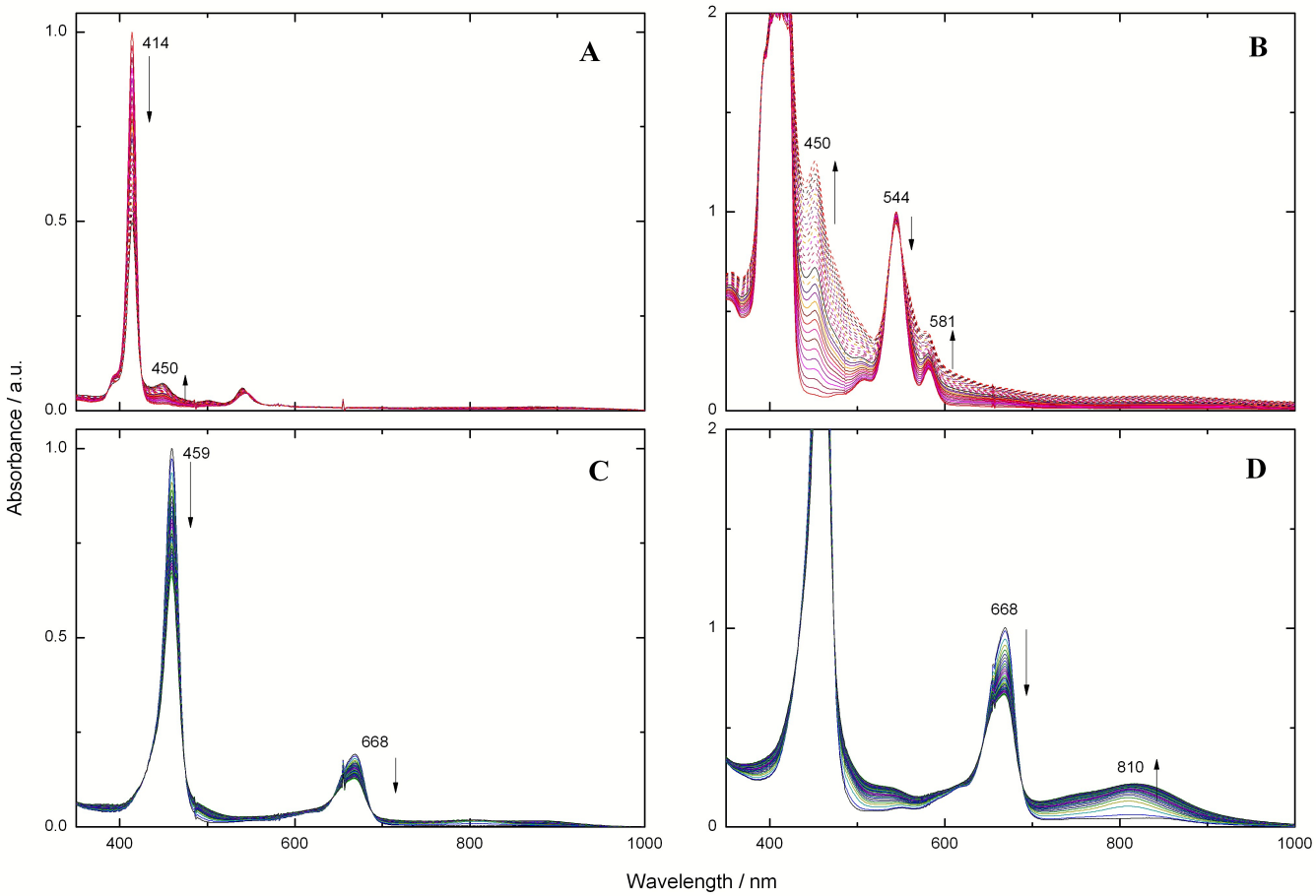

Fig. 13 Normalized UV-vis spectra recorded every four seconds during oxidative electrolysis in 0.1 M Bu_4NPF_6/THF at a platinum mesh electrode for **4** A) 20 μM and B) 0.66 mM, and **9** C) 20 μM and D) 0.44 mM. Electrolysis time: 120 s.

View Article Online
DOI: 10.1039/C6CP01026A

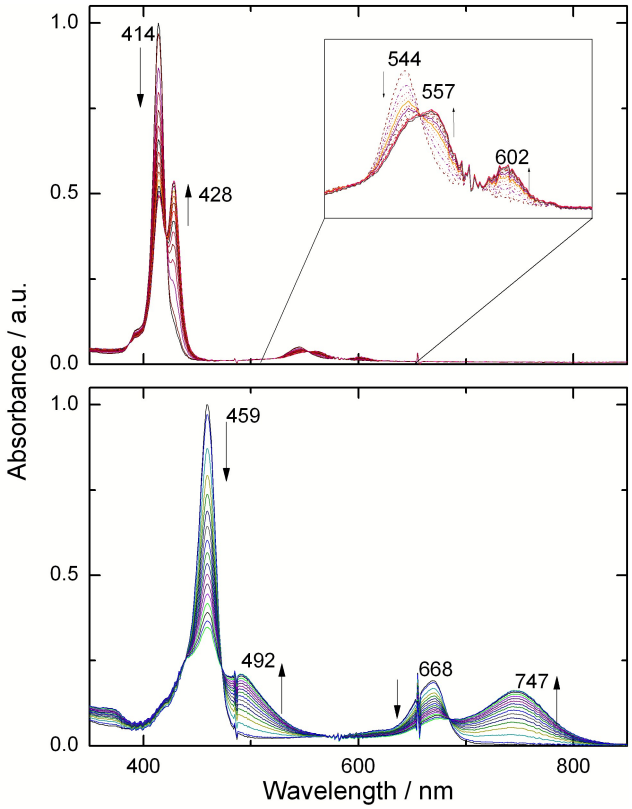

Fig. 14 Normalized UV-vis spectra recorded every four seconds during reductive electrolysis in 0.1 M Bu_4NPF_6/THF at a platinum mesh electrode for 20 μM **4** (top), and **9** (bottom). Electrolysis time: 120 s.

Porphyrin radical anions are expected upon electrolysis on the potential corresponding to the first reduction wave. Potential was set at approximately 100 mV more negative than the cathodic peak in *ca.* 20 μM solutions. Reductive electrolysis of **4** results in two isosbestic points in the spectra: the first one corresponding to the simultaneous disappearance of the Soret band (414 nm) and the appearance of a Soret-like band (428 nm), the second is for the Q band at 544 nm that gradually decreases giving place to a small band at 557 nm (Fig. 14). There are no lower energy bands corresponding either to the formation of the radical anion or a phlorin.[10, 61–64] Porphyrin **9** presents the characteristics of metalloporphyrin radical anions, that is, decrease and broadening of the Soret band at 459 nm, increase of a band at 492 nm, the diminishing Q band at 668 nm, and, most remarkably, the appearance of a new broad band at 747 nm.[59,63,64] For the carbazole-substituted porphyrin, the high absorbance from 650 to 800 nm of the radical anion is in accordance with the quenching of the ECL that results in the asymmetric transients (Fig. 10).

Experimental

General

Reagents for the synthesis were purchased from commercial sources and used as received unless otherwise indicated below. Column chromatography was performed on silica gel 60 (0.2-0.5 mm, Merck). Thin-layer chromatography (TLC) was carried out on aluminum sheets coated with silica gel 60 F_{254} (Merck); plates were inspected under UV light. For the electrochemical experiments, anhydrous tetrahydrofuran (THF, ≥ 99.9%, inhibitor free), obtained from Sigma-Aldrich, was used as received. Electrochemical grade tetrabutylammonium hexafluorophosphate (Bu_4NPF_6, ≥ 99.0%) was purchased from Fluka and dried at 60 °C under vacuum prior to use. For ECL experiments tetrahydrofuran (THF) was purified as previously reported,[65] analytical grade Bu_4NPF_6, and benzoyl peroxide (BPO) were obtained from Sigma-Aldrich.

NMR spectra were obtained on an Agilent 400 MR (400 MHz) or a Bruker Avance III (700 MHz) spectrometer; chemical shifts are reported in parts per million downfield from tetramethylsilane resonance, which was used as an internal reference. Electron ionization mass spectrometry (EI-MS) was performed on a Thermo-Electron DFS (Double Focus Sector) spectrometer; for gas chromatography-mass spectrometry (GC-MS) analyses, an Agilent 6890N series gas chromatograph (DB-5MS capillary column) coupled to a LECO Pegasus 4D time-of-flight spectrometer was used. Electrospray ionization mass spectrometry (ESI-MS) was carried out on a Waters SQD system in positive mode: capillary 4.5 kV; cone 200 V; desolvation temperature 80 °C; desolvation gas 200 L/h. High-resolution electrospray ionization mass spectrometry (HR-ESI-MS) was performed on a Thermo QExactive Plus spectrometer in positive mode: spray voltage 4.0 kV; capillary temperature 300 °C, sheath gas flow rate 50, auxiliary gas 15.

Synthetic procedures

2,2'-dipyrromethane (1).[66] Paraformaldehyde (1.3285 g, 44.24 mmol) and freshly distilled pyrrole (306 mL, 4.424 mol) under nitrogen were heated at 50 °C for 10 minutes. $InCl_3$ (978.5 mg, 4.42 mmol) was added, and the solution was stirred for 1 h and then cooled. NaOH (981 mg, 24.5 mmol) and alumina (1 g) were added, the mixture was stirred for 1 h, then filtered. Excess pyrrole was removed by distillation yielding a brown sticky crude that was purified by column chromatography (silica gel, hexane: ethylacetate 8:2). A white crystalline solid was obtained (3.582 g, 55.4% yield). R_f= 0.28 (hexane: ethylacetate 8:2), m.p.= 70–71 °C.

4-octyloxybenzaldehyde (2).[67] 4-hydroxybenzaldehyde (6.15 g, 50.39 mmol), 1-bromooctane (8.6 mL, 49.8 mmol), and potassium carbonate (27.73 g, 200 mmol) were dissolved in DMF (125 mL). The mixture was stirred at 100 °C for 4 hours and then cooled for 30 minutes until it reached room temperature. Cold water was added (100 mL) and then the crude product was extracted into $CHCl_3$; the organic phase was washed with saturated brine and dried under reduced pressure. The product was purified by column chromatography (silica gel, hexane: ethylacetate 8:2). A liquid lightly yellowish compound was obtained (8.269 g, 70.6% yield). R_f = 0.62 (hexane: ethylacetate 8:2), ^{1}H NMR (400 MHz, $CDCl_3$, TMS, ppm): δ= 9.879 (1H, s), 7.825 (2H, d, J_1= 8.8 Hz, J_2= 2.2 Hz), 6.989 (2H, d, J_1= 8.8 Hz, J_2= 2.2 Hz), 4.039 (2H, t, J= 6.8 Hz), 1.831 (H_a) and 1.794 (H_b) (2H, t, J= 6.8 Hz), 1.241 – 1.502 (10H, m), 0.890 (3H, t, J= 6.8 Hz).

DOI: 10.1039/C6CP01025A

5,15-bis-[4-(octyloxy)phenyl]-porphyrin (3).[68] 2,2'-dipyrromethane (1.46 g, 10 mmol) and 4-octyloxybenzaldehyde (2.35 g, 10 mmol) were dissolved in CH_2Cl_2 (1100 mL), purged with nitrogen, and then trifluoroacetic acid (TFA, 667 µL) was added. The solution was protected from light and stirred for 3 h at room temperature under nitrogen. 2,3-dichloro-5,6-dicyano-1,4-benzoquinone (DDQ, 3.48 g, 15.33 mmol) was added, stirring continued for 3 more hours. Triethylamine (TEA, 3.3 mL) was added and the mixture was filtered through alumina. Solvent was removed under reduced pressure. Crude product was purified by column chromatography (deactivated silica gel 1% TEA, toluene) and a purple solid was obtained. (725 mg, 10.1 % yield), m.p. > 250 °C. ^{1}H NMR (400 MHz, $CDCl_3$, TMS, ppm): δ= 10.299 (2H, s, *meso*), 9.390 (4H, d, *J*=4.8 Hz, pyrrolic), 9.117 (4H, d, *J*=4.8 Hz, pyrrolic), 8.177 (4H, d, *J*=8.4 Hz, -CH Ph), 7.342 (4H, d, *J*=8.4 Hz, -CH Ph), 4.289 (4H, t, *J*=6.8 Hz, O-CH_2-), 2.017 (4H, q, *J*=6.4 Hz, -CH_2-), 1.658 (4H, q, *J*=6.8 Hz, -CH_2-), 1.383-1.546 (16H, m, -CH_2-), 0.957 (6H, t, *J*=6.4 Hz, -CH_3). ESI-MS: *m/z* 718 (M^+) (calc. for $C_{48}H_{54}N_4O_2$ m/z 718.4 M^+).

{5,15-bis-[4-(octyloxy)phenyl]-porphyrinato}zinc (II) (4).[68] Porphyrin 3 (490.6 mg, 682 µmol) was dissolved in DMF (30 mL). Zinc acetate (1.5 g, 6.81 mmol) was added and the solution was refluxed for 1 h. Mixture was cooled and distilled water (30 mL) was added. Product was filtered and further washed with cold water. A bright pink solid was obtained (489.6 mg, 91.7% yield, 6.5% overall yield). R_f = 0.84 (hexane: $CHCl_3$ 2:8), m.p. > 250 °C. HR-ESI-MS: *m/z* 780.3375 (M^+) (calc. for $C_{48}H_{52}N_4O_2Zn$ m/z 780.3382 M^+, –0.9 ppm).

{5,15-dibromo-10,20-bis-[4-(octyloxy)phenyl]-porphyrinato}zinc (II) (5).[68] Porphyrin 4 (489.6 mg, 625.8 µmol) was dissolved in $CHCl_3$ (25 mL) and cooled to 0 °C. N-bromosuccinimide (NBS, 227.5 mg, 1.28 mmol) was added and the solution stirred for 5 minutes. Adding acetone (3 mL) quenched the reaction. Solvent was removed under reduced pressure; crude was washed with water and filtered, yielding a purple solid, green when dissolved, that was used without further purification. An analytical sample was purified. m.p. > 250 °C, HR-ESI-MS: *m/z* 936.1619 (M^+), 875.3605 (M^+–Zn), 795.4504 (M^+–Zn–Br) (calc. for $C_{48}H_{50}N_4O_2Br_2Zn$ m/z 936.1592 M^+, +2.9 ppm)

3-iodocarbazole (6).[69] Carbazole (2.50 g, 15 mmol), and potassium iodide (1.66 g, 10 mmol) in acetic acid glacial (41 mL) were stirred and heated at 100 °C; potassium iodate (1.64 g, 7.7 mmol) was added. The mixture was refluxed for 2 h and then cooled to room temperature. A solid precipitated by adding cool water, it was filtered and further washed with water, resulting in a brown solid (3.81 g). Part of the crude (1 g) was purified by column chromatography (silica gel hexane: ethylacetate 9:1) yielding a white crystalline solid (461.1 mg, 40%); R_f = 0.23 (hexane: ethylacetate 9:1) m.p.= 195-196 °C. ^{1}H NMR (400 MHz, $CDCl_3$, TMS, ppm): δ= 8.386 (1H, dd, J_1= 1.6 Hz, J_2= 0.4 Hz), 8.060 (1H, br s), 8.024 (1H, dd, J_1= 7.8 Hz, J_2= 0.4 Hz), 7.662 (1H, dd, J_1= 8.4 Hz, J_2= 1.6 Hz), 7.426 – 7.443(2H, m), 7.212 – 7.268 (2H, m). GC–MS: *m/z* 293 (M^+), 166 (M^+ – I) (calc. for $C_{12}H_8IN$ m/z 293 M^+).

3-[2-(trimethylsilyl)ethynyl]carbazole (7).[70] 3-yodocarbazole (152.1 mg, 519 µmol), $PdCl_2(PPh_3)_2$ (18.2 mg, 26 µmol), and CuI (4.9 mg, 26 µmol) were placed in a two-neck round bottom flask; air inside the flask was flushed with a nitrogen current and then it was placed inside a glovebox. TEA (1.0 mL) and THF (14 mL) were added to the flask; the solution was stirred for 5 min., then trimethylsilylacetylene (102 µL, 716 µmol) was added. After 2 h at room temperature, an extra 185 µL (1.29 mmol) of trimethylsilylacetylene were added. Mixture was stirred for a total of 5.5 h. TEA and THF were evaporated using nitrogen current outside the glovebox. A brownish solid was obtained; it was purified by column chromatography (silica gel hexane: $CHCl_3$ 1:1) yielding a beige product (89.9 mg, 65.9%). R_f = 0.52 (hexane: ethylacetate 8:2), ^{1}H NMR (400 MHz, $CDCl_3$, TMS, ppm): δ=8.223 (1H, s), 8.096 (1H, br s, N-H), 8.041 (1H, dd, J_1= 8.0 Hz, J_2= 0.8 Hz), 7.531 (1H, dd, J_1= 8.4 Hz, J_2= 1.6 Hz), 7.414 – 7.437 (2H, m), 7.338 (1H, d, *J*= 8.4 Hz), 7.226 – 7.274 (1H, m), 0.290 (9H, s, Si-CH_3).

3-ethynylcarbazole (8).[71] 3-[2-(trimethylsilyl)ethynyl]carbazole (89.9 mg, 341.8 µmol) and potassium carbonate (236.2 mg, 1.709 mmol), were refluxed on benzene: methanol 1:1 (30 mL) for 30 min. Solvents were removed under reduced pressure. Crude was extracted into $CHCl_3$ and washed with water. A white solid (59.9 mg, 91.7% yield) was obtained. It was not further purified as it decomposes on silica. R_f = 0.50 (hexane: ethylacetate 8:2) ^{1}H NMR (400 MHz, $CDCl_3$, TMS, ppm): δ= 8.241 (1H, s), 8.127 (1H, br s, N-H), 8.054 (1H, d, *J*= 8.0 Hz), 7.550 (1H, dd, J_1= 8.4 Hz, J_2= 1.6 Hz), 7.440 (2H, dd, J_1= 3.2 Hz, J_2= 0.8 Hz), 7.370 (1H, d, *J*= 8.4 Hz), 7.237 – 7.283 (1H, m), 3.061 (1H, s). EI-MS: *m/z* 191 (M^+) (calc. for $C_{14}H_9N$ m/z 191 M^+).

{5,15-bis-(carbazol-3-yl-ethynyl)-10,20-bis-[4-(octyloxy)phenyl]-porphinato}-zinc (II) (9).[72] 3-ethynylcarbazole (59.9 mg, 314 µmol), and porphyrin 5 (140.4 mg, 149.3 µmol) were placed in a two-neck round bottom flask; air inside the flask was flushed with nitrogen current and then it was placed inside a glovebox. Tri(o-tolyl)phosphine (P(*o*-tol)$_3$, 54.5 mg, 179.2 µmol), tris(dibenzylideneacetone)dipalladium(0) ($Pd_2(dba)_3$, 20.5 mg, 22.4 µmol), TEA (1.0 mL), and of THF (5 mL) were added to the flask. Mixture was stirred for 1.5 h at 30 °C and filtered through silica. Solvent was evaporated and the crude was purified by column chromatography (silica gel hexane: THF 7:3). A green solid was obtained (78.1 mg, 45.1% yield, 2.6% overall yield). R_f = 0.34 (hexane: THF 7:3), m.p. > 250 °C, ^{1}H NMR (700 MHz, d_8-THF, TMS, ppm): δ= 10.68 (2H, s, -NH carbazole), 9.85 (4H, d, *J*= 4.3 Hz, pyrrolic), 8.94 (4H, d, *J*= 4.3 Hz, pyrrolic), 8.85 (2H, s, -CH carbazole), 8.31 (2H, d, *J*= 7.3 Hz, -CH carbazole), 8.15 (4H, d, *J*= 8.2 Hz, -CH Ph), 8.12 (2H, d, *J*= 8.1 Hz, -CH carbazole), 7.68 (2H, d, *J*= 8.2 Hz, -CH carbazole), 7.54 (2H, d, *J*= 8.2 Hz, -CH carbazole), 7.47 (2H, t, *J*= 7.5 Hz, -CH carbazole), 7.38 (4H, d, *J*= 8.2 Hz, -CH Ph), 7.29 (2H, t, *J*= 7.3 Hz, -CH carbazole), 4.34 (4H, t, *J*=6.2 Hz, O-CH_2-), 2.04 (4H, m, -CH_2-), 1.73 (4H, m, -CH_2-), 1.58 (4H, m, -CH_2-), 1.2-1.5 (m, -CH_2-), 1.01 (6H, t, *J*=7.0 Hz, -CH_3). ^{13}C NMR (175 MHz, d_8-THF, TMS, ppm): δ= 13.54 (-CH_3), 20.41, 22.67, 26.31, 29.42, 29.81, 31.95 (-CH_2-), 67.83

View Article Online
DOI: 10.1039/C6CP01926A

(O-CH_2-), 93.27 (C-*meso*-ethynyl), 97.7, 97.8 (C-ethynyl), 110.91, 110.76 (C1, C8 carbazole), 119.16, 114.43 (C3, C6 carbazole), 123.66, 120.28 (C4, C5 carbazole), 129.01, 125.86 (C2, C7 carbazole), 123.59, 122.98 (C4a, C4b carbazole), 140.80 (C9a, C8a carbazole), 122.19 (C-*meso*-Ph), 135.38, 112.38 (C2, C3 Ph), 135.38 (C1 Ph), 159.15 (C4 Ph), 131.86, 130.22 (β-C pyrrolic), 151.87, 150.16 (α-C pyrrolic); ^{13}C NMR assignments are supported by HSQC and HMBC data (Spectra shown in ESI). HR-ESI-MS: *m/z* 1158.4521 (M^+) (calc. for $C_{76}H_{66}N_6O_2Zn$ m/z 1158.4539 M^+, –1.5 ppm).

Absorption and Emission Spectra

Absorption spectra were acquired at room temperature on THF with a Varian Cary 5 spectrophotometer. For the steady-state fluorescence experiments, deoxygenated 0.2 µM porphyrin THF solutions on a homemade airtight cell were used; emission and excitation spectra were recorded on a Varian Cary Eclipse spectrofluorimeter at room temperature. Fluorescence yields were measured as described by Marcaccio and coworkers.[73]

Electrochemical Cells, Electrodes, and Instruments.

Cyclic Voltammetry. Experiments were carried out in a three-electrode jacketed cell. Temperature of the jacketed cell was controlled with a circulating bath at −5 °C. Solutions were purged with ultra high purity argon (Infra), passed through a gas bubbler with the solvent before reaching the cell. The working electrode was a 0.3 cm diameter glassy carbon electrode with an effective area of 0.077 cm^2. Before each measurement, the working electrode was polished with 0.05 µm alumina paste (Buehler), rinsed with water, sonicated in distilled water and dried with a tissue. The reference electrode was an $Ag/AgNO_3$ electrode; a silver wire immersed in 0.10 M Bu_4NPF_6/ 0.01 M silver nitrate/acetonitrile at room temperature (nonisothermal operation). The reference electrode was separated from the test solution by a porous Vycor frit from Bioanalytical Systems. The potential of the reference electrode was periodically measured with respect to the reversible ferrocenium/ferrocene couple, and was found to be 171 mV in Bu_4NPF_6 0.1 M/THF. All potentials reported in this work are referred to the Fc^+/Fc couple unless otherwise stated. An Autolab PGSTAT 302 potentiostat-galvanostat was used for the cyclic voltammetry experiments.

Digital Simulations. Simulations were performed using DigiElch 4F, a software for digital simulation of common electrochemical experiments (http://www.digielch.de).[74] When matching simulations to the experimental voltammograms, the objective was to find the single set of parameter values that provided the best average fit between simulation and experiment for the entire range of concentrations and scan rates employed. This means that a simulation at a given scan rate might be improved by some variation of one or more parameter values, but this could lower the average goodness-of-fit for the entire set of voltammograms. The total uncompensated resistance in Bu_4NPF_6 0.1 M/THF at −5 °C (R_u = 3500 Ω) was determined as previously described. [75]

ECL experiments. An electrochemical cell of airtight design with high-vacuum glass (or Teflon) stopcocks fitted with Viton O-rings was used, spherical joints with O-rings served as connections between the cell and the vacuum line or Schlenk flask that contains the solvent.[76] The working electrode consisted of a platinum side oriented 2 mm diameter disk sealed in glass while the counter electrode was a platinum spiral and the reference electrode was a quasi-reference silver wire. THF was distilled into the cell by a trap-to-trap procedure; the pressure measured in the cell prior to the distillation was around 10^{-5} mbar. Bu_4NPF_6 was used as supporting electrolyte, and the experiments were carried out at room temperature. In a given solution, two or three records were made to check the temporal stability of the system investigated. The annihilation reaction was performed by pulsing the working electrode between the first oxidation and the first reduction peak potential of the complex with a pulse width of 0.1 s. When co-reactant was used the potential was stepped form 0 V to a negative value where both porphyrin and BPO are reduced. The ECL signal generated by performing the potential step program was measured with a photomultiplier tube (PMT, Hamamatsu R4220p) placed a few millimetres from the cell, and in front of the working electrode, inside a darkbox. A voltage in the range 250-750 V was supplied to the PMT. The light/current/voltages curves were recorded by collecting the preamplified PMT output signal (by a ultra-low noise Acton Research model 181) with the second input channel of the ADC module of the AUTOLAB instrument.

ECL spectra were recorded by inserting the same PMT in a dual exit monochromator (Acton Research model Spectra Pro2300i) and collecting the signal as described above. Photocurrent detected at the PMT was accumulated for 1-3 seconds, depending on the emission intensity, for each monochromator wavelength step (usually 1 nm). Entrance and exit slits were fixed to the maximum value of 3 mm.

The ECL yield is defined as the photons emitted per redox event, which is related to the total electrical charge involved in the generation of the reactants. Thus, the ECL efficiency can be rigorously estimated by the annihilation method and obtained by chronoamperometric experiment using equation 2.[49]

$$\phi_{ECL} = \phi^o_{ECL}\left(\frac{IQ^o}{I^oQ}\right) \qquad (2)$$

Where ϕ^o_{ECL} is the ECL efficiency of the standard under the same experimental conditions, *I* and *I°* are the integrated ECL intensity of the species and the standard systems, *Q* and *Q°* the faradaic charges (in Coulombs) passed for the investigated species and the standard species, respectively. It has been estimated that the ECL efficiency can be confidently given with an error of ±15%. In order to obtain the ECL yields, measurements of a standard ECL system were performed under similar experimental conditions as those used for the

View Article Online
DOI: 10.1039/C6CP01926A

porphyrins. The chosen standard was $[Ru(bpy)_3]^{2+}$ (bpy=bipyridine) which is among the most efficient ECL systems.[77] The ECL intensity ratio ($I_{porphyrin}/I_{[Ru(bpy)3]2+}$) was determined and the ECL yield of the porphyrins can be directly obtained considering the reported ECL annihilation efficiency of 5% for $[Ru(bpy)_3]^{2+}$ (Fig. 8S, ESI).

Spectroelectrochemistry. Spectroelectrochemical experiments were performed on a thin-layer quartz electrochemical cell (path length 1 mm, BASi) with a three-electrode arrangement consisting of an optically transparent platinum minigrid as working electrode, a Pt wire as counter electrode and $Ag/AgNO_3$ as reference. The cell was paired to a BASi Epsilon potentiostat-galvanostat and the spectra were obtained using an Agilent 8453 UV-vis spectrophotometer. Measurements were carried out on deoxygenated solutions in Bu_4NPF_6 0.1 M/THF at room temperature.

Conclusions

Two A_2B_2 porphyrins were synthesized, porphyrin **9**, with two ethynylcarbazol units at the *meso* positions, and porphyrin **4**, having two free *meso* positions. Absorption and emission bands of **9** are red-shifted compared to **4**; also the lower energy Q band of porphyrin **9** has a much larger extinction coefficient than any of the Q bands of **4**. Additionally, the $E_{1/2}$ values for the one-electron oxidation and reduction waves show that the formation of the radical ions of **9** requires less energy than for porphyrin **4**. These observations demonstrate that the ethyne group connecting the carbazol and porphyrin units allows for an effective increase on the conjugation of the porphyrin ring.

Extending the conjugation of the porphyrin ring also improves the stability of the radical ions. Digital simulation reveals that the radical cation and the radical anion of porphyrin **9** are more stable than those of **4**. On the other hand, the lack of substituents at the *meso* positions leads to a dimerization reaction of the radical cation that is most likely followed by the formation of a polymer or oligomer, as shown by the higher concentration electrolysis experiments.

Electrochemiluminescence of the porphyrins was achieved *via* the radical ion annihilation mechanism by pulsing the potential between the first oxidation and first reduction values, as well as through the coreactant BPO. Both porphyrins show asymmetric ECL transients, for porphyrin **4** these observations were correlated with the formation of oligomers or polymers following the initial dimerization step; spectroelectrochemistry investigations, together with controlled potential electrolysis, support these findings. Porphyrin **9** displays very similar intensity ECL transients compared to **4**, this unexpectedly low ECL emission can be rationalized by the self-absorption of the intense Q band and also by the intense absorption band observed during the one-electron reduction of **9** that matches with the emission of the porphyrin.

Acknowledgements

We thank to the Dirección General de Apoyo al Personal Académico (DGAPA-UNAM, PAPIIT IN213615) for the financial support for this research. E.K.G-M is grateful to CONACyT for her PhD grant and to Programa de Doctorado en Ciencias Químicas, UNAM. We thank Dra. Isabel Rivero, and Georgina Duarte Lisci for the mass spectrometry experiments; Iván Puente Lee for the SEM microscopy; Dra. Minerva Monroy Barreto, and Dra. Beatriz Quiroz for recording the ^1H and ^{13}C NMR spectra. This study made use of UNAM's NMR lab: LURMN at Instituto de Química-UNAM, which is funded by CONACyT (project 0224747) and UNAM.

References

1 M. Biesaga, K. Pyrzyńska and M. Trojanowicz, *Talanta*, 2000, **51**, 209–224.
2 T. Aida and S. Inoue, in *The Porphyrin Handbook vol. 6*, eds. K. M. Kadish, R. Guilard and K. M. Smith, Academic Press, San Diego, 2000, p. 132.
3 M. Jurow, A. E. Schuckman, J. D. Batteas and C. M. Drain, *Coord. Chem. Rev.*, 2010, **254**, 2297–2310.
4 T. Higashino and H. Imahori, *Dalton Trans.*, 2015, **44**, 448–463.
5 J. Kesters, P. Verstappen, M. Kelchtermans, L. Lutsen, D. Vanderzande and W. Maes, *Adv. Energy Mater.*, 2015, **5**, 1–20.
6 C. M. Drain, J. T. Hupp, K. S. Suslick, M. R. Wasielewski and X. Chen, *J. Porphyr. Phthalocyanines*, 2002, **6**, 243–258.
7 T. Tanaka and A. Osuka, *Chem. Soc. Rev.*, 2014, **44**, 943–969.
8 H. L. Anderson, *Chem. Commun.*, 1999, 2323–2330.
9 K. Susumu, P. R. Frail, P. J. Angiolillo and M. J. Therien, *J. Am. Chem. Soc.*, 2006, **128**, 8380–8381.
10 J. Rawson, P. J. Angiolillo and M. J. Therien, *Proc. Natl. Acad. Sci. U. S. A.*, 2015, **112**, 13779–13783.
11 M.-C. Kuo, L.-A. Li, W.-N. Yen, S.-S. Lo, C.-W. Lee and C.-Y. Yeh, *Dalton Trans.*, 2007, 1433–1439.
12 S. M. LeCours, S. G. DiMagno and M. J. Therien, *J. Am. Chem. Soc.*, 1996, **118**, 11854–11864.
13 S. M. LeCours, H. W. Guan, S. G. DiMagno, C. H. Wang and M. J. Therien, *J. Am. Chem. Soc.*, 1996, **118**, 1497–1503.
14 P. K. Goldberg, T. J. Pundsack and K. E. Splan, *J. Phys. Chem. A*, 2011, **115**, 10452–10460.
15 M. O. Senge, M. Fazekas, M. Pintea, M. Zawadzka and W. J. Blau, *Eur. J. Org. Chem.*, 2011, **2011**, 5797–5816.
16 H. Qin, L. Li, F. Guo, S. Su, J. Peng, Y. Cao and X. Peng, *Energy Environ. Sci.*, 2014, **7**, 1397.
17 Y. Q. Wang, X. Li, B. Liu, W. J. Wu, W. H. Zhu and Y. S. Xie, *RSC Adv.*, 2013, **3**, 14780–14790.
18 K. M. Kadish, E. Van Caemelbecke and G. Royal, in *The Porphyrin Handbook vol. 8*, eds. K. M. Kadish, R. Guilard and K. M. Smith, Academic Press, San Diego, 2000, pp. 1–114.
19 E. K. Galván-Miranda, G. Zaragoza-Galán, E. Rivera, M. Aguilar-Martínez and N. A. Macías-Ruvalcaba, *Electrochim. Acta*, 2014, **148**, 266–275.
20 A. J. Bard, J. D. Debad, J. K. Leland, G. B. Sigal, J. L. Wilbur

and J. N. Wohlstadter, *Encycl. Anal. Chem.*, 2006, 1–8.
21 N. R. Armstrong, R. M. Wightman and E. M. Gross, *Annu. Rev. Phys. Chem.*, 2001, **52**, 391–422.
22 W. Miao, *Chem. Rev.*, 2008, **108**, 2506–2553.
23 M. Hesari and Z. Ding, *J. Electrochem. Soc.*, 2016, **163**, H3116–H3131.
24 Y. Zhao, R. Zhang, Y. Xu, H. Qi, X. Chen and C. Zhang, *J. Electroanal. Chem.*, 2015, **739**, 28–35.
25 N. E. Tokel, C. P. Keszthelyi and A. J. Bard, *J. Am. Chem. Soc.*, 1972, **94**, 4872–4877.
26 N. E. Tokel-Takvoryan and A. J. Bard, *Chem. Phys. Lett.*, 1974, **25**, 235–238.
27 P. Canty, L. Väre, M. Håkansson, A.-M. Spehar, D. Papkovsky, T. Ala-Kleme, J. Kankare and S. Kulmala, *Anal. Chim. Acta*, 2002, **453**, 269–279.
28 E. M. Gross, N. R. Armstrong and R. M. Wightman, *J. Electrochem. Soc.*, 2002, **149**, E137.
29 T. R. Long and M. M. Richter, *Inorg. Chim. Acta*, 2005, **358**, 2141–2145.
30 D. J. Vinyard, S. Swavey and M. M. Richter, *Inorg. Chim. Acta*, 2007, **360**, 1529–1534.
31 A. Bolin and M. M. Richter, *Inorg. Chim. Acta*, 2009, **362**, 1974–1976.
32 F.-C. Chen, J.-H. Ho, C.-Y. Chen, Y. O. Su and T.-I. Ho, *J. Electroanal. Chem.*, 2001, **499**, 17–23.
33 D. Luo, B. Huang, L. Wang, A. M. idris, S. Wang and X. Lu, *Electrochim. Acta*, 2015, **151**, 42–49.
34 G.-Y. Zhang, S.-Y. Deng, X.-J. Zhang and D. Shan, *Electrochim. Acta*, 2016, **190**, 64–68.
35 C. Sooambar, V. Troiani, C. Bruno, M. Marcaccio, F. Paolucci, A. Listorti, A. Belbakra, N. Armaroli, A. Magistrato, R. De Zorzi, S. Geremia and D. Bonifazi, *Org. Biomol. Chem.*, 2009, **7**, 2402–13.
36 K. Susumu, T. Shimidzu, K. Tanaka and H. Segawa, *Tetrahedron Lett.*, 1996, **37**, 8399–8402.
37 T. Ogawa, Y. Nishimoto, N. Yoshida, N. Ono and A. Osuka, *Angew. Chem. Int. Ed.*, 1999, **111**, 140–142.
38 C. H. Devillers, D. Lucas, A. K. D. Dime, Y. Rousselin and Y. Mugnier, *Dalton Trans.*, 2010, **39**, 2404–2411.
39 M. Gouterman, G. H. Wagnière and L. C. Snyder, *J. Mol. Spectrosc.*, 1963, **11**, 108–127.
40 P. J. Spellane, M. Gouterman, A. Antipas, S. Kim and Y. C. Liu, *Inorg. Chem.*, 1980, **19**, 386–391.
41 P. N. Taylor, A. P. Wylie, J. Huuskonen and H. L. Anderson, *Synthesis*, 1998, 986–989.
42 V. S. Lin, S. G. DiMagno and M. J. Therien, *Science*, 1994, **264**, 1105–1111.
43 L. R. Milgrom and G. Yahioglu, *Tetrahedron Lett.*, 1995, **36**, 9061–9064.
44 M. Uttamlal and A. S. Holmes-Smith, *Chem. Phys. Lett.*, 2008, **454**, 223–228.
45 M. M. Sartin, F. Camerel, R. Ziessel and A. J. Bard, *J. Phys. Chem. C*, 2008, **112**, 10833–10841.
46 K. M. Omer, S. Ku, K. Wong and A. J. Bard, *J. Am. Chem. Soc.*, 2009, **131**, 10733–10741.
47 K. Suzuki, A. Kobayashi, S. Kaneko, K. Takehira, T. Yoshihara, H. Ishida, Y. Shiina, S. Oishi and S. Tobita, *Phys. Chem. Chem. Phys.*, 2009, **11**, 9850.
48 A. Lukaszewicz, J. Karolczak, D. Kowalska, A. Maciejewski, M. Ziolek and R. P. Steer, *Chem. Phys.*, 2007, **331**, 359–372.
49 A. J. Bard, *Electrogenerated Chemiluminescence*, Marcel Dekker, New York, First., 2004.
50 A. B. Nepomnyashchii, M. Bröring, J. Ahrens, R. Krüger and A. J. Bard, *J. Phys. Chem. C*, 2010, **114**, 14453–14460.
51 N. L. Ritzert, T.-T. Truong, G. W. Coates and H. D. Abruña, *J. Phys. Chem. C*, 2014, **118**, 924–932.
52 M. M. Sartin, F. Camerel, R. Ziessel and A. J. Bard, *J. Phys. Chem. C*, 2008, **112**, 10833–10841.
53 M. Hesari, J.-S. Lu, S. Wang and Z. Ding, *Chem. Commun.*, 2015, **51**, 1081–1084.
54 G. Valenti, A. Fiorani, S. Di Motta, G. Bergamini, M. Gingras, P. Ceroni, F. Negri, F. Paolucci and M. Marcaccio, *Chem. Eur. J.*, 2015, **21**, 2936–2947.
55 M. Hesari, S. M. Barbon, V. N. Staroverov, Z. Ding and J. B. Gilroy, *Chem. Commun.*, 2015, **51**, 3766–3769.
56 J. Rosenthal, A. B. Nepomnyashchii, J. Kozhukh, A. J. Bard and S. J. Lippard, *J. Phys. Chem. C*, 2011, **115**, 17993–18001.
57 M. Shen, J. Rodríguez-López, J. Huang, Q. Liu, X. H. Zhu and A. J. Bard, *J. Am. Chem. Soc.*, 2010, **132**, 13453–13461.
58 J. Fajer, D. C. Borg, A. Forman, D. Dolphin and R. H. Felton, *J. Am. Chem. Soc.*, 1970, **92**, 3451–3459.
59 P. Neta, *J. Phys. Chem. B*, 1981, **85**, 3678–3684.
60 A. K. D. Dime, C. H. Devillers, H. Cattey, B. Habermeyer and D. Lucas, *Dalton Trans.*, 2012, **41**, 929–936.
61 J. Mack and M. J. Stillman, *J. Porphyr. Phthalocyanines*, 2001, **5**, 67–76.
62 J. G. Lanese and G. S. Wilson, *J. Electrochem. Soc.*, 1972, **119**, 1039–1043.
63 G. L. Closs and L. E. Closs, *J. Am. Chem. Soc.*, 1963, **85**, 818–819.
64 R. A. Reed, R. Purrello, K. Prendergast and T. G. Spiro, *J. Phys. Chem.*, 1991, **95**, 9720–9727.
65 C. Bruno, R. Benassi, A. Passalacqua, F. Paolucci, C. Fontanesi, M. Marcaccio, E. A. Jackson and L. T. Scott, *J. Phys. Chem. B*, 2009, **113**, 1954–1962.
66 J. K. Laha, S. Dhanalekshmi, M. Taniguchi, A. Ambroise and J. S. Lindsey, *Org. Process Res. Dev.*, 2003, **7**, 799–812.
67 N. Xiang, Y. Liu, W. Zhou, H. Huang, X. Guo, Z. Tan, B. Zhao, P. Shen and S. Tan, *Eur. Polym. J.*, 2010, **46**, 1084–1092.
68 M. J. Plater, S. Aiken and G. Bourhill, *Tetrahedron*, 2002, **58**, 2405–2413.
69 A. Dyatkin, Universal Display Corporation, USA, Pat. WO2012048266 A1, 2012.
70 M. Kanai, T. Hirano, I. Azumaya, I. Okamoto, H. Kagechika and A. Tanatani, *Tetrahedron*, 2012, **68**, 2778–2783.
71 E. Rivera, M. Belletête, X. Xia Zhu, G. Durocher and R. Giasson, *Polymer*, 2002, **43**, 5059–5068.
72 A. Ryan, A. Gehrold, R. Perusitti, M. Pintea, M. Fazekas, O. B. Locos, F. Blaikie and M. O. Senge, *Eur. J. Org. Chem.*, 2011, **2011**, 5817–5844.
73 G. Valenti, C. Bruno, S. Rapino, A. Fiorani, E. a. Jackson, L. T. Scott, F. Paolucci and M. Marcaccio, *J. Phys. Chem. C*, 2010, **114**, 19467–19472.

View Article Online
DOI: 10.1039/C6CP01926A

74 M. Rudolph, *J. Electroanal. Chem.*, 2003, **543**, 23–39.
75 N. A. Macías-Ruvalcaba and D. H. Evans, *J. Phys. Chem. B*, 2005, **109**, 14642–14647.
76 L. Della Ciana, S. Zanarini, R. Perciaccante, E. Marzocchi and G. Valenti, *J. Phys. Chem. C*, 2010, **114**, 3653–3658.
77 W. L. Wallace and A. J. Bard, *J. Phys. Chem.*, 1979, **83**, 1350–1357.